RESEARCH ARTICLE - EARTH SCIENCES

Supplementary Studies of Textural and Mineralogical Changes in Reservoir and Caprocks from Selected Potential Sites Suitable for Underground CO₂ Storage

Magdalena Wdowin · Radosław Tarkowski · Wojciech Franus

Abstract The purpose of this article is to present the results of the study, which are supplementary to the results obtained earlier by Tarkowski and Wdowin in Oil Gas Sci Technol 66:137–150, 2011, on the impact of CO₂ on rocks in order to determine the effects of carbon dioxide sequestration. Its aim was to observe changes, in textural parameters (BET surface area, pore size distribution) and mineral composition, resulting from experimental exposure of reservoir and caprock samples to CO₂ at subsurface conditions. The samples were Jurassic (sandstones, dolostone) and Cretaceous (sandstones, limestone) rocks of central Poland. The experiments were conducted in the presence of CO₂ and brines for a 3-month period at simulated formation conditions ($T = 55\,^{\circ}C$, $P = 12$ MPa—Jurassic, $T = 45^{\circ}C$, $P = 10$ MPa—Cretaceous) using a laboratory apparatus. An increase in BET surface area was observed in sandstones after the experiment. The analysis of dolostone revealed a decrease in the BET values and a slight increase of this parameter was observed in limestone. The clay fraction in the dolostone showed the presence of kaolinite and micas in mineral composition. Illite–smectite from the clay fraction of the limestone showed a shift of the d(001) basal spacing towards lower values due to the replacement of calcium by sodium (from Jackson treatment) in the interlayer space. This shift proves the occurrence of smectite layers. The mineral compositions and surface parameters of the studied reservoir and caprocks indicate that rock properties changed very differently.

M. Wdowin (✉) · R. Tarkowski
The Mineral and Energy Economy Research Institute of The Polish Academy of Sciences, Wybickiego 7, 31-261 Kraków, Poland
e-mail: mwdowin@gmail.com

W. Franus
Department of Geotechnics, Civil Engineering and Architecture Faculty, Lublin University of Technology, Nadbystrzycka 40, 20-618 Lublin, Poland

الخلاصة

إن الغرض الأساسي من هذه المقالة هو عرض نتائج الدراسة التي تُعدّ مكملة للنتائج التي تم الحصول عليها في وقت سابق من قبل تاركوسكي وودوين (2011) عن أثر ثاني أكسيد الكربون في الصخور من أجل تحديد الآثار المترتبة على احتجاز ثاني أكسيد الكربون. إنها تهدف إلى مراقبة التغيرات في المتغيرات التكوينية (مساحه BET السطحية، توزيع حجم المسام) والتركيب المعدني، والناتج من جراء التعرض التجريبي للخزان وعينات صخور الذروة إلى ثاني أكسيد الكربون في ظروف تحت السطح. وعينات الصخور هي من العصر الجوراسي (الحجر الرملي، والحجر الرسوبي المعدني) والعصر الطباشيري (الحجر الرملي والحجر الجيري) من وسط بولندا. وقد أجريت التجارب في وجود ثاني أكسيد الكربون والمحاليل الملحية لفترات مدة ثلاثة أشهر في ظروف تشكيل محاكاة (درجة الحرارة = 55 مئوية، الضغط = 12 ميجا باسكال ـ العصر الجوراسي، درجة الحرارة = 45 مئوية، الضغط = 10 ميجا باسكال ـ العصر الطباشيري) باستخدام أجهزة المختبر. وقد لوحظ زيادة في مساحة BET السطحية في الحجر الرملي بعد التجربة. وكشف تحليل الحجر الرسوبي المعدني انخفاضا في قيم BET ، ولوحظ وجود زيادة طفيفة من هذا المعامل في الحجر الجيري. وأظهر الجزء الطيني في الحجر الرسوبي المعدني وجود الكولنيت وميكا في التركيب المعدني. وأظهرت الإليت ـ سمكتايت من الجزء الطيني من الحجر الجيري إزاحة من د (001) تباعد اساسي نحو قيم أقل بسبب استبدال الكالسيوم بالصوديوم (من معالجة جاكسون) في الفضاء البيني. وتثبت هذه الإزاحة جود طبقات سمكتايت. وتشير التراكيب المعدنية ومعاملات السطح للخزان المدروس وصخور الذروة إلى أن خواص الصخور قد تغيرت بشكل مختلف جدا.

1 Introduction

Carbon dioxide is one of the main greenhouse gases [1]. Because of the increase in the rate of global industrial activity,

Springer

its concentration in the air continues to rise rapidly. Methods and technologies for the reduction of anthropogenic release of CO_2 to the atmosphere are being currently developed [2]. A promising method seems to be CCGS technology (Carbon Capture and Geological Storage) that relies on the storage of CO_2 in underground geological structures [3–5], where CO_2 has a contact with brine (saline aquifer) and rocks. This would be another usage of geological formations and aquifers that are often used to extract hydrocarbons and saline waters for desalination [6] and to store treated sewage effluents [7].

One of the numerous problems concerning the storage of CO_2 in geological structures is its impact on rocks and reservoir fluids, as recognised during previous studies on the suitability of rocks and geological structures for underground CO_2 storage [8,9]. Once injected, carbon dioxide interacts with the rocks and reservoir fluids: it dissolves in reservoir liquids [2,3], reacts with minerals of the rock matrix [10], undergoes hydrodynamic trapping [11] and, if the sealing is not perfect, can leak into overlying lithologies [12], or ultimately to the surface. This contribution aims to address the phenomena occurring during CO_2 injection and after the completion of the processes that may affect the capacity of the CO_2 storage reservoir or the sealing properties of the caprocks. Understanding the interaction processes between CO_2, rock and reservoir fluids is also important for optimizing the process of CO_2 injection into underground reservoirs. Considering these phenomena when planning CO_2 storage projects reduces risks of gas leakage from the underground reservoir, and consequent failure of the storage operation [13].

The main aim of this contribution is to evaluate changes in the rocks that result from the interaction between brine, CO_2 and reservoir and caprock samples, and to answer the question as to whether and how such interactions affect the properties of reservoir (sandstones) and cap (carbonate) rocks. The results of the study are also presented so as to check if the supplementary research shown in the article has any significance in the experiments of this kind. Moreover, the authors also intend to verify whether the preparation of the samples and the time during which the interaction between rock, CO_2 and brine takes place are of any importance for the purpose of the experiment.

2 Materials and Experimental Methods

2.1 Materials

Eight samples were studied. They were collected from drill cores from boreholes Pagórki IG 1 (sample Nos. 1–4) and Brzeœæ Kujawski IG 2 and IG 3 (sample Nos. 5–8) located in the Polish Lowlands (near Włocławek, Central Poland, Fig. 1). Two reservoir horizons selected for underground

CO_2 storage (Table 1) were chosen [14–17]: a Lower Cretaceous horizon (quartzose sandstones, sample Nos. 2–4) and a Lower Jurassic horizon (quartzose sandstones, sample Nos. 6–8). Caprock samples were also collected (Cretaceous limestone, sample No. 1; Jurassic dolostone, sample No. 5). Borehole samples were located in the Gopło (name of the borehole: Pagórki IG 1) and Brześć Kujawski (names of the boreholes: Brześć Kujawski IG 2 and Brześć Kujawski IG 3) anticlines (names of boreholes are taken from locations of these wells). Both locations were proposed as potential sites suitable for underground CO_2 storage.

2.2 Laboratory Tests

A setup, which simulates natural formation conditions during CO_2 injection, i.e. elevated pressure (P) and temperature (T), was designed to study the influence of CO_2 on Mesozoic reservoir and caprocks (see [18]).

The experimental apparatus (Fig. 2) was composed of four stainless steel (4H13) reactors with 100 mm inner diameter and 230 mm length, each with a capacity of $V = 1.80$ dm^3. The apparatus was also equipped with a KBC-65G heating chamber (WAMED company) and connected to a CO_2 supply.

The drill core samples (4 cm diameter—drilled parallel to drill cores, c.a. 10 cm height each) (around 400 g) were placed in the sealed reactors filled with 1.5 dm^3 of artificial brine (different for Cretaceous and Jurassic rocks, Table 2). The remaining capacity of the reactors (around 0.15 dm^3) was filled with CO_2. The reactors as well as samples' pore space were not evacuated before charging of carbon dioxide. Then, the reactors were placed into the heating cabin.

The experiment consisted of three parts: the impact of CO_2 on brine alone (so-called blank experiment), the impact of CO_2 on Cretaceous rocks in the presence of brine, and the impact of CO_2 on Jurassic rocks in the presence of brine. Each experiment for the Cretaceous and Jurassic rocks lasted three months. The aim of the experiments was to observe short-term interactions between brines and the samples. The in situ conditions established for the Cretaceous and Jurassic rocks were as follows: $P = 10$ MPa ± 1 MPa and $T = 45\,°C$ $\pm 4.5\,°C$ for the Pagórki region; and $P = 12$ MPa ± 1 MPa and $T = 55\,°C \pm 5.5\,°C$ for the Brześć Kujawski region. For the blank experiment, which lasted 2 weeks, the conditions were: $P = 12$ MPa ± 1 MPa and $T = 55\,°C \pm 5.5\,°C$.

2.3 Methods

In order to analyze the processes within the rocks after CO_2 injection, textural and detailed mineralogical-petrographic investigations were performed on the rock samples before and after the tests that were conducted in the presence of carbon dioxide and brines. The following parameters, which
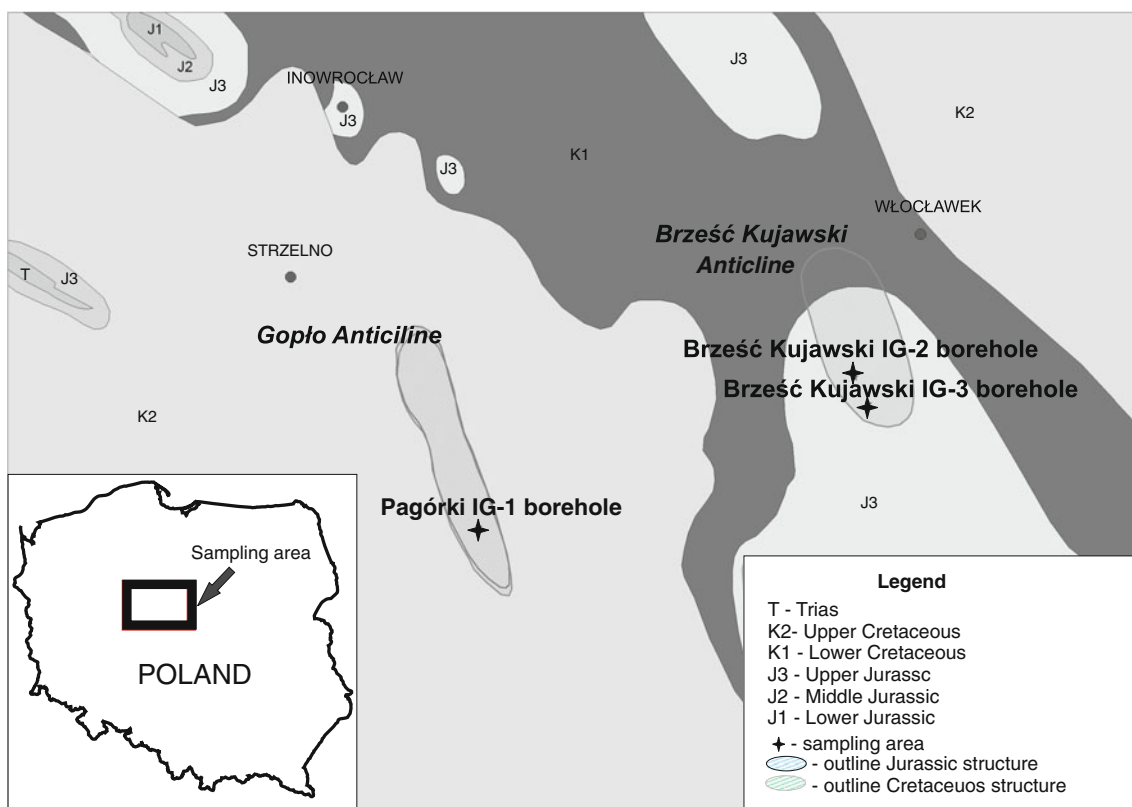
Fig. 1 Geological map showing main geological structures and sampling areas (after Tarkowski and Wdowin [18])

Table 1 Rock material collected for investigations

| Sample	Type of material	Remarks	Depth (m)
No. 1	Limestone (Upper Cretaceous)	Caprock	865–870
No. 2	Sandstone (Lower Cretaceous)	Reservoir rock	1,025–1,029
No. 3	Sandstone (Lower Cretaceous)	Reservoir rock	1,056–1,059
No. 4	Sandstone (Lower Cretaceous)	Reservoir rock	1,072–1,079
No. 5	Dolostone (Middle Jurassic)	Caprock	1,019–1,027
No. 6	Sandstone (Middle Jurassic)	Reservoir rock	1,129–1,130
No. 7	Sandstone (Lower Jurassic)	Reservoir rock	1,210–1,211
No. 8	Sandstone (Lower Jurassic)	Reservoir rock	1,309–1,310
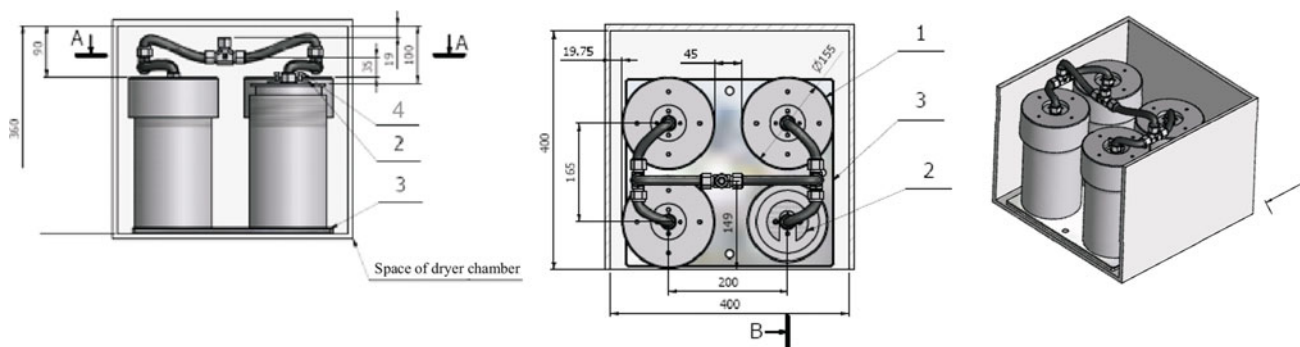
Fig. 2 Scheme of the experimental setup: *1* reactor; *2* sealing ring; *3* the supporting plate reactors; *4* CO_2 supplying pipe

Table 2 Physicochemical parameters of initial Cretaceous and Lower Jurassic brines

Marked component	Content in initial sample (Cretaceous)	Content in initial sample (Jurassic)
Reaction (pH)	7.4	7.4
Conductivity (20 °C) (μS/cm)	46,750	6,671
Specific weight (g/cm^3)	1.022	1.033
Dry residue (g/l)	30.948	47.1
Chloride (mg Cl/l)	17,106	27,387
Sulphate (mg SO_4/l)	721	460
Bicarbonate (mg HCO_3/l)	292	589
Carbonate (mg CO_3/l)	0.00	0.00
Calcium (mg Ca/l)	874	1,094
Magnesium (mg Mg/l)	292	331
Sodium (mg Na/l)	10,442	16,322
Potassium (mg K/l)	122	181

can be sensitive to the changes caused by CO_2, were measured: specific BET surface area, average diameter of pores, and pore size distribution (ranging from 0.2 to 300 nm)[17]. For mineralogical investigations, SEM-EDS and transmitted light observations, as well as XRD analyses were carried out. Additional XRD analyses of the sediments deposited at the bottom of the reactors after the experiments were conducted.

In this supplementary study, we used similar experimental procedures and the same samples as were previously used by Tarkowski and Wdowin [18].

2.3.1 Determination of N_2-BET Surface Area and Textural Parameters

Textural investigations of the specific surface areas and the associated pore size distribution were performed using Micromeritics ASAP 2405 analyser.

The values of specific BET surface area and pore size distribution were determined on the basis of the shape of adsorption/desorption isotherms of nitrogen vapour at 77 K [19]. BET surface area was calculated based on Brunauer–Emmett–Teller's multilayer adsorption theory [20] at P/P_0 between 0.01 and 0.3 (P equilibrium pressure, P_0 saturation pressure).

Total pore volume, V_p, was determined from the volume of adsorbed nitrogen at the pressure of $P/P_0 = 0.98$. Pore volume distribution was calculated using the Barret–Joyner–Hallenda (BJH) method based on the combination of the modified Kelvin equation and statistical adsorbed film thickness. Pore diameters, D_p, were calculated according to the formula $D_p = 4V_p/S_{BET}$.

2.3.2 Mineralogical and Petrographic Characterization

Microscopic observations in transmitted light were carried out using a Nikon Eclipse 6000Pol polarizing microscope.

X-ray diffraction analyses of the rock and the clay fraction were performed using a PHILIPS X'Pert APD diffractometer (with a PW 1870 generator and PW 3020 vertical goniometer). Cu Kα_1 graphite-monochromatized radiation ($\lambda = 0.154062$ nm), using a curved monochromator, was applied. The analyses were performed within the angle range of 2°–64° 2 Θ with the velocity 0.02°/1 s, accelerating voltage 40 KV and a current of 30 mA [21].

The clay fraction was separated from carbonates. Before the separation of the <2 μm fraction, the samples underwent the Jackson's procedure [22]. The successively separated fractions were saturated with sodium in order to create monocation form of samples. This was done in suspension. After the disappearance of chloride ions the samples were dialyzed, homogenized and dried. Subsequently, oriented mounts on glass slides [23] were made by means of the sedimentation method. X-ray diffraction patterns of the preparations were recorded in air-dry conditions, after saturation with ethylene glycol vapour (12 h, temperature 60 °C) and after heating (min. time 1 h) at the temperatures of 330 and 550 °C (see [23]).

X-ray diffraction was also used to analyse the mineral composition of the sediments formed at the bottom of the reactors after the experiment. For this purpose, a DRON-3.0 diffractometer was used. The analyses were performed within the angle range of 3−74 ° 2Θ. Cu Kα_1 ($\lambda = 0.154062$ nm) radiation and a nickel filter were employed. The operating voltage was 34 kV, current 30 mA, recording step by step with step 2 $\Theta = 0.05$ ° and counting time 1 s/step.

Observations of the mineral composition and rock sample surface before and after the experiment were made using a Hitachi S-4700 field emission scanning electron microscope equipped with the Noran Vantage dispersive spectroscopy system and YAG BSE detector. SEM-EDS observations were also performed on standard polished thin sections (0.025 mm thick).

3 Research Results

3.1 Previous Investigations

The previous research conducted by Tarkowski and Wdowin [18], during which the same samples and procedures were utilised, concerned the observation of changes in the quantitative mineralogical composition of rock samples (planimetric analysis), physico-chemical parameters of brines, petrophysical parameters (porosity, permeability) before and after the experiment.

When it comes to the mineralogical researches the results have shown minor variations (mainly in the amount of the individual minerals in planimetric analysis) where most of them may have been the result of not using exactly the same sample before and after the experiment. The authors explained that some changes resulted from the application of destructive methods to determine parameters (i.e. XRD analysis) in some cases, but they also indicated that the samples were collected from the same drill core intervals, so their petrophysical parameters and mineralogical characteristics should be very similar.

The experiment conducted by authors did not reduce the sealing quality of the caprocks, on the contrary, their sealing properties improved (decreased porosity and decreased threshold diameter in the case of sample No. 1).

Physicochemical parameters of brines, such as specific conductance, total solids content, specific gravity and post-reaction total solids content remained unchanged.

3.2 Detailed Investigation of Pore Space Texture

3.2.1 Cretaceous and Jurassic Sandstone Samples (Caprock Sample Nos. 2–4, 6–8)

Specific BET surface areas before experiments (Table 3) vary from 0.31 to 0.79 m^2/g. Pore size distributions (PSD) in sandstone samples measured within the range 0.2–300 nm (Figs. 3 and 4) show variability (homogeneous distribution for sample Nos. 2, 4, 6, 7; bimodal distribution for sample No. 3; polymodal distribution for sample No. 8) in the interval from 2.5 to 15 nm. Pores of 3 nm diameter are predominant. According to the ASAP texture analysis and IUPAC classification [24], rocks are characterised by Type IV isotherms, indicating their micro/mesopore texture. The hysteresis loop type is H3/H2 (Figs. 3 and 4). The rocks have predominantly blind spherical and ink bottle-shaped pores [25]. The average diameters of pores (ranging from 0.2 to 300 nm) before

experiment of the Cretaceous and Jurassic samples are presented in the Table 3.

Considering the instrument measurement errors of an apparatus in textural analysis, i.e. BET surface areas and average pore diameters (Table 3), it was found that these results for sandstone did not change significantly after the experiment. In these analyses it is also necessary to take into account that the results of the measurements depend on many factors: i.e. sample preparation, degassing, weighing, bath temperature stability, and purity of gases used in the analysis, etc.

More accurate results are obtained for materials with large surface area and volume. The results obtained after the experiments, revealed that the biggest changes were observed for samples with very small BET surface area. This is most likely due to the previously described errors, which influence the reliability of the measurement, where accuracy of the manifold transducer is ± 0.1 % of full scale reading (includes non-linearity, hysteresis and non-repeatability) and linearity is ± 0.05 % of full scale reading.

The specific BET surface area of the Cretaceous and Jurassic samples increased after the experiments, except for the sample Nos. 3 (Cretaceous) and 6 (Jurassic), where the BET values decreased. PSD for sample Nos. 2, 3, 4, 7 shows bimodal distribution of pores; and for sample Nos. 6 and 8, a polymodal distribution. The percentage of pores (ranging from 0.2 to 300 nm) remained at the same level and the pores of 3 nm diameter remained prevalent. These rock samples are mesoporous. The shapes of both sorption isotherms and hysteresis loop did not change significantly after the tests. The average diameter values of pores (ranging from 0.2 to 300 nm) decreased in all of the sandstone samples.
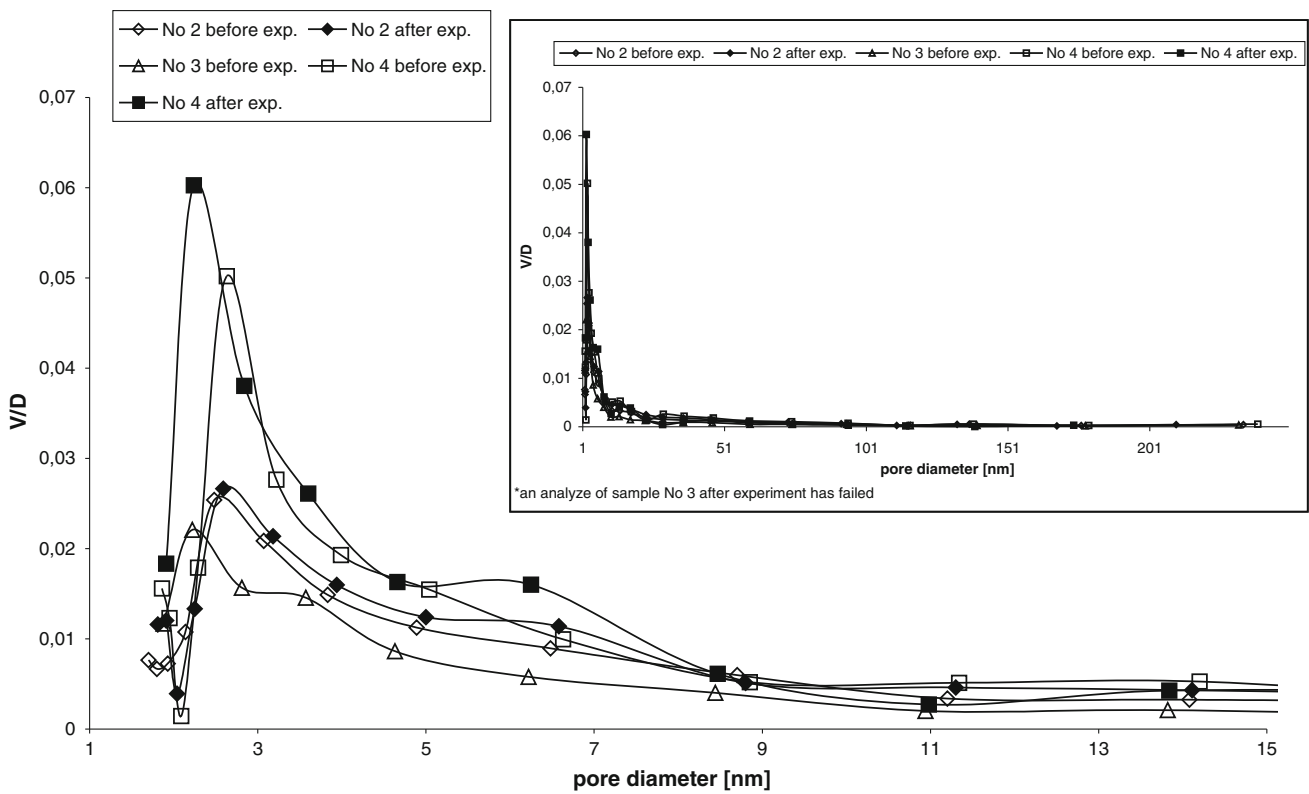
3.2.2 Upper Cretaceous Limestone Sample (Sample No. 1)

Sample No. 1 is a limestone of specific BET surface area 5.04 m^2/g, which is higher than that of the sandstone samples.

Table 3 Values of specific BET surface area (in m^2/g) and average pores diameter (ranging from 0.2 to 300 nm) measured in the samples before and after the experiment all treatments

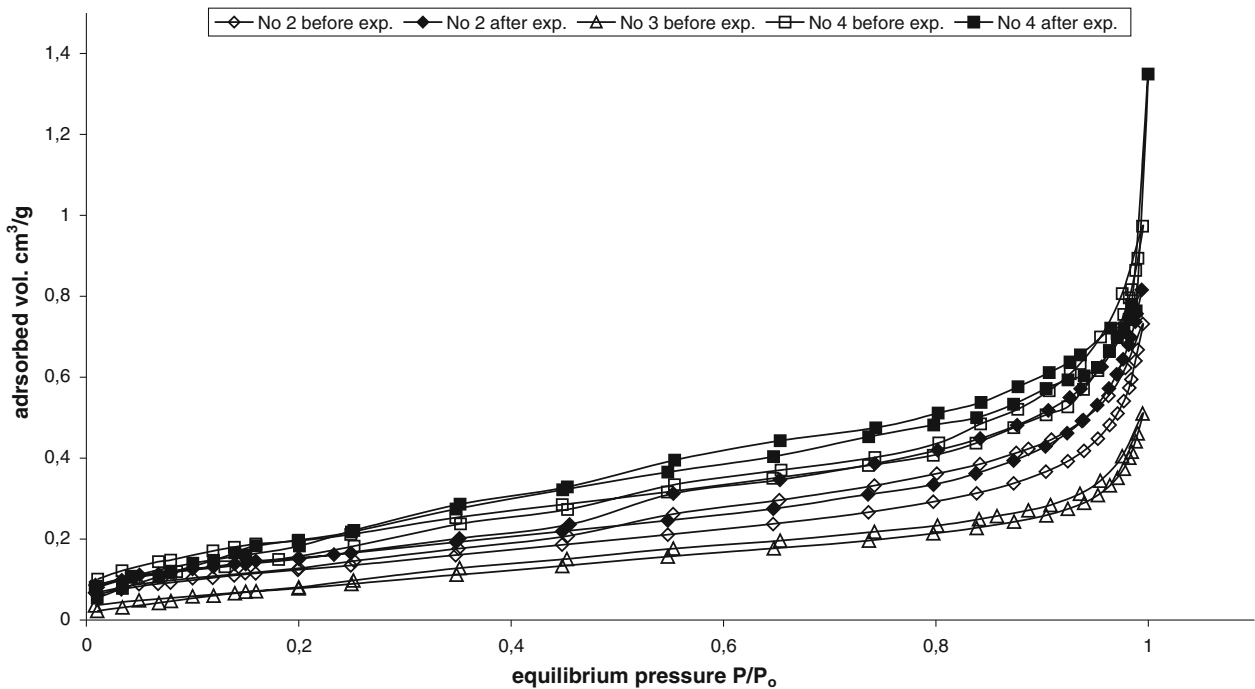| Sample	BET surface area before the experiment	BET surface area after the experiment	Average pore diameter before the experiment (nm)	Average pore diameter after the experiment (nm)
No. 1	5.04	5.48	8.259	7.330
No. 2	0.45	0.56	8.207	7.766
No. 3	0.31	0.17	8.240	6.275
No. 4	0.71	0.79	7.051	5.901
No. 5	11.10	7.92	6.726	6.858
No. 6	0.71	0.68	12.922	9.507
No. 7	0.39	0.56	10.148	9.486
No. 8	0.35	0.44	11.496	10.868

Fig. 3 Pore size distribution and N_2 sorption/desorption isotherm of Cretaceous sandstone samples (sample Nos. 2–4) before and after the experiment

ASAP textural analysis shows higher sorption values than those obtained in the sandstone samples. This is due to the higher values of specific surface area of the rock. The analysis

pores distribution (ranging from 0.2 to 300 nm) indicates that the dominant pore size ranges within the interval of 2–25 nm (Fig. 5), with the most frequent diameter of approximately
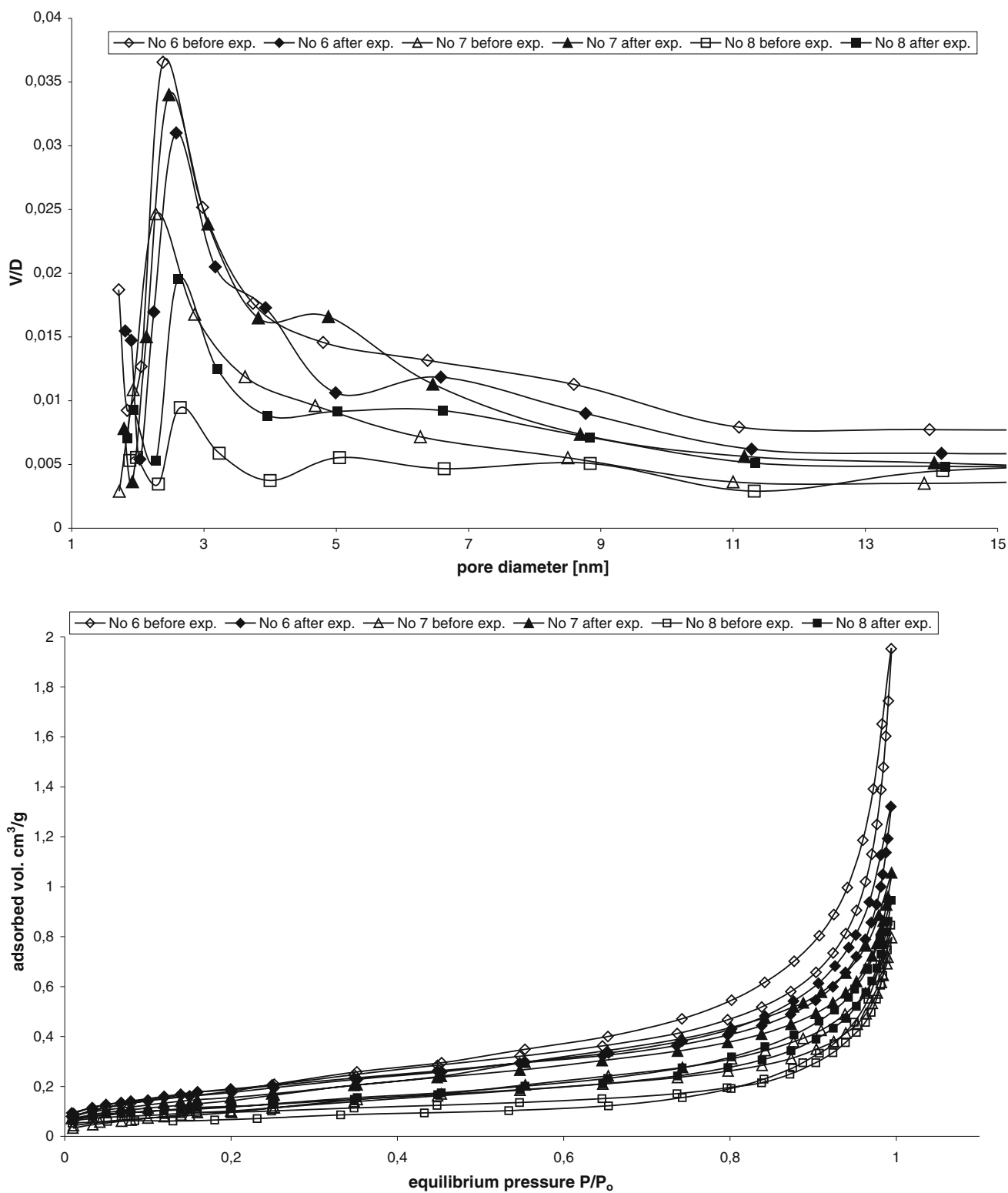
Fig. 4 Pore size distribution and N$_2$ sorption/desorption isotherms of Jurassic sandstone samples (sample Nos. 6–8) before and after the experiment

3 nm. Thus, the limestone is a micro/mesoporous carbonate rock. This sample represents Type IV sorption isotherm, and the hysteresis loop (Fig. 5) is H3/H2 indicating blind spherical and ink bottle shaped pores [25]. The average diameter of pores (ranging from 0.2 to 300 nm) measured before the experiment was 8.259 nm.
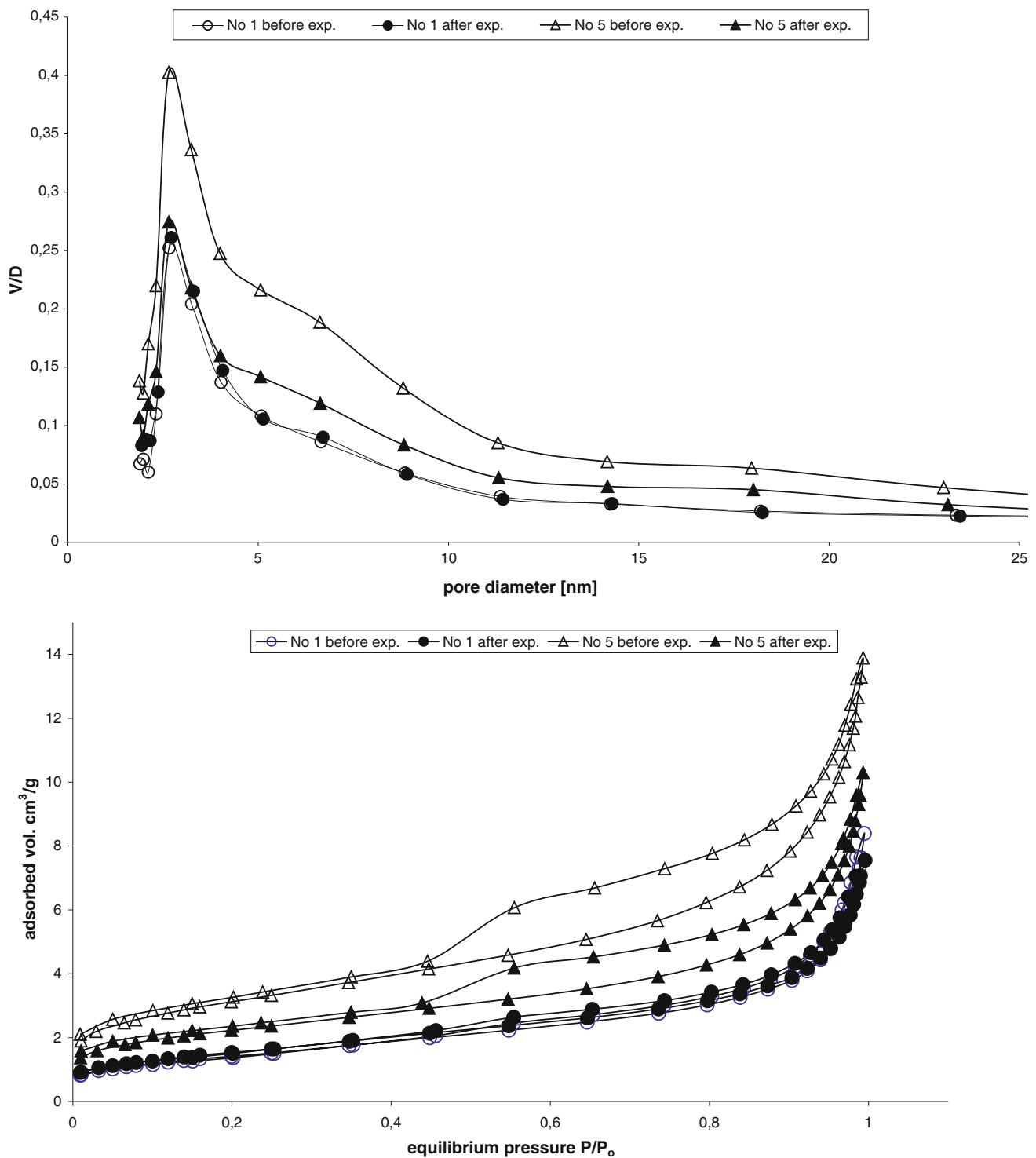
Fig. 5 Pore size distribution and N_2 sorption/desorption isotherms of carbonates (sample Nos. 1 and 5) before and after the experiment

No significant changes in visual inspection and measured parameters were observed in sample No. 1 after the experiment. The value of specific BET surface area increased slightly to 5.48 m²/g. In case of pores (ranging from 0.2 to 300 nm) diameter values, only a slight decrease were observed.

Comparison of the shapes of N_2 desorption isotherms (hysteresis loops) did not reveal any changes in the curve shapes and adsorbed nitrogen volume. The average diameter of pores after the experiment decreased to 7.330 nm.

3.2.3 Middle Jurassic Dolostone Sample (Sample No. 5)

The value of specific BET surface area for sample No. 5 is 11.10 m^2/g. The analysis of pores distribution (ranging from 0.2 to 300 nm) reveals that the rock is a micro/mesoporous carbonate rock, with predominant pore size of 2–25 nm (Fig. 5). The most frequent diameter was approximately 3 nm. The rock is characterised by Type IV isotherms and Type H2 hysteresis loop of the smallest pores (Fig. 5). The average pore diameter before the experiment was 6.726 nm. The dolostone sample did show some changes in these parameters after the experiment. The value of specific BET surface area decreased to 7.92 m^2/g. The presence of brine and CO_2 did not affect either the structure or the percentage of pores (ranging from 0.2 to 300 nm) in diameter. The average diameter of pores (ranging from 0.2 to 300 nm) increased slightly to 6.858 nm.

3.3 Mineralogical and Petrographical Characterization

3.3.1 Cretaceous and Jurassic Sandstone Samples (Sample Nos. 2–4, 6–8)

The non-treated samples collected from the reservoirs are represented by variously grained quartzose sandstones, dominated by quartz grains. Rare feldspars grains, clay minerals forming thin coatings on quartz grains, opaque minerals (pyrite, rutile), accumulations of brownish iron compounds, muscovite, kaolinite (often authigenic) and glauconite (sample No. 2) were observed in the Cretaceous samples. Sample Nos. 2, 6 and 7 also contain rock fragments. Kaolinite and kaolinite–apatite aggregates and apatite and gypsum grains were found in sample No. 6. Sample No. 8 also contains organic matter.

All the samples were cemented, but with differently developed siliceous and interstitial cement. Locally, there is interstitial clay-siliceous cement. The rocks are occasionally porous and in sample Nos. 2 and 3 the pores are filled with a clay-carbonate mixture. Sample Nos. 6 and 8 locally contain clay or clay-ferruginous (sample No. 6) cements and the pores in the former sample are also filled with carbonate-clay, clay (kaolinite) and clay-ferruginous material. The pores in sample Nos. 7 and 8 are commonly filled with silica (chalcedony), locally with sericite, illite and iron compounds (sample No. 7) or kaolinite (sample No. 8).

Mineralogical analysis of the samples performed after the experiments showed no significant changes in the grain framework, cementation and pore space filling cements. In the case of sample No. 2, a decrease of the carbonate cement quantity nearly to zero was observed. XRD analysis of sample No. 4 revealed a small amount of pyrite, not detected previously. XRD analyses of all the samples showed the presence of halite, that is an artefact after drying and not washing samples after experiments.

3.3.2 Upper Cretaceous Limestone Sample (Sample No. 1)

Original and non-treated rock is composed of micritic limestone containing abundant bioclasts, with sporadic detrital quartz and mica grains. Spherical or oval accumulations of opaque minerals (pyrite, iron oxides) occur locally. Various types of calcite, depending on the origin, and pure calcitic micrite without clay minerals were also observed. A variable concentration of clay minerals and compounds of iron are intergrown in large calcite grains.

SEM observations confirmed the presence of crystalline calcite, bioclasts and micritic groundmass intergrown in place by large accumulations of clay minerals or by calcite recrystallization.

XRD analysis of original sample showed that the mineral composition of the rock is predominantly calcite. The XRD pattern also exhibited weak reflections characteristic for illite-type clay minerals.

The following clay minerals and mixed-layer clay minerals were identified based on literature information [23,26]. The clay fraction separated from sample No. 1 (Fig. 6) contained mainly illite/smectite mixed-layer minerals (a broad peak within the d-spacing range of 5.0–5.5), small amount of kaolinite and quartz. In the case of illte–smectite, slight shifts of reflections towards lower values were observed, probably resulting from the replacement of calcium by sodium (from Jacksons' treatment) at interlayer sites. This shift is because swelling properties of smectite.

After the experiment, SEM analysis showed organic remains and crystalline calcite that is occasionally replaced by pyrite. Dispersed or large accumulations of clay minerals occur between the calcite grains. After the experiment, the XRD pattern also revealed the presence of subordinate quartz and clay minerals, and a small reflection related to halite.

Overall, mineralogical investigations did not reveal any significant changes to the limestone due to the exposure to CO_2-rich fluids during the experiments.

3.3.3 Lower Jurassic Dolostone Sample (Sample No. 5)

This rock is a finely crystalline marly and ferruginous dolostone containing very fine dolomite crystals with surfaces stained red by iron oxides. The accumulations of clay minerals, probably kaolinite impregnated by iron oxides, occur between the dolomite grains. The fine-grained, mainly clay-carbonate groundmass also contains quartz grains, pyrite and rare muscovite flakes. Quartz grains are commonly angular and randomly distributed or arranged in laminae. Pyrite occurs as irregular crystals and variously sized framboidal forms. Dolomitic recrystallization was observed around muscovite flakes. Iron oxides are variably distributed, from disseminated to large accumulations and laminates. There are also irregular, occasionally rhombohedral ferruginous

Fig. 6 X-ray diffraction pattern of the clay fraction from the sample No. 1 before and after the experiment
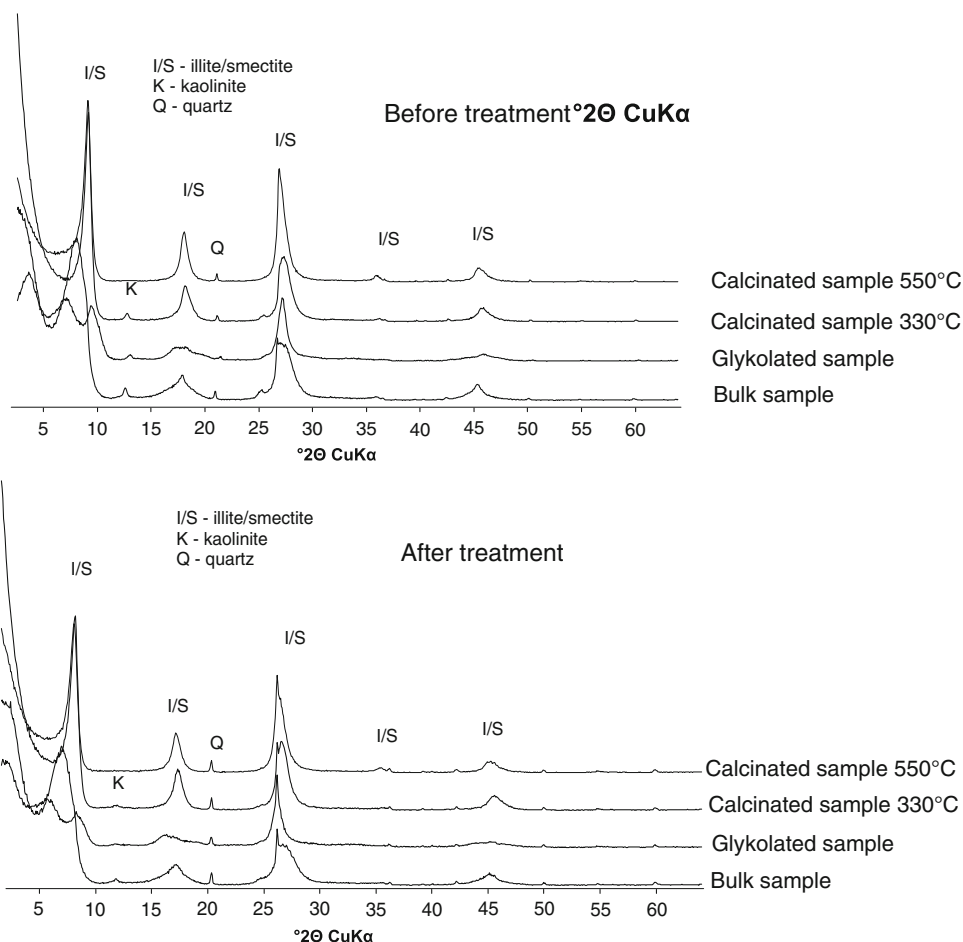
dolomite grains with a fine-grained matrix of clay minerals (stained by iron oxides) between them. The Fe concentration tends to increase towards the edges of dolomite crystals, producing a zonal structure of the grains. The clay matrix between the grains is stained by iron oxides.

The XRD analysis showed that ferruginous dolomite/ankerite (diffraction reflections of these minerals occupy the same position) are the main component of the rock. In addition to dolomite, quartz, kaolinite and illite-type minerals were observed. The clay fraction separated from this sample (Fig. 7) contains abundant kaolinite as well as small amounts of chlorite.

After the exposure to CO_2-rich fluids, only small changes were observed in transmitted light, SEM and XRD analyses of the rock samples. XRD analysis of the clay fraction (Fig. 7) revealed large amounts of kaolinite and micas, and a small proportion of chlorite.

3.4 XRD Analysis of the Sediments

Some amounts of sediments were accumulated at the bottom of the reactors during the experiments, as a result of the reaction between CO_2 and brine. The sediment was observed in the reactors containing rock samples, it occurred during the blank experiment as well. The sediment was analysed via X-ray diffraction in order to determine its basic mineral composition. The analysis was also intended to check whether the sediment originated from the rock samples, or whether it represents newly formed minerals resulting from the interactions between the rock, brine and CO_2 at elevated pressure and temperature.

The analysis of sediment formed at the bottom of reactor during the blank test with the Lower Cretaceous brine did not give reliable results (Fig. 8). Increased background intensity in the XRD pattern made the reflections of individual minerals hard to distinguish. The sediment was mostly composed of carbonates (calcite, aragonite) and sulphates (gypsum, anhydrite and jarosite). Feldspars, mica and halite were observed in smaller quantities.

In the blank experiment in which a Lower Jurassic brine was used, XRD diffraction results (Fig. 8) were difficult to interpret because of high background intensity. The composition of the sediment revealed reflections related to carbonate minerals (probably calcite, aragonite and siderite), as well as anhydrite. There were also peaks apparently related to quartz, goethite and halite. However, the results of the analy-

Fig. 7 X-ray diffraction pattern of the clay fraction from the sample No. 5 before and after the experiment
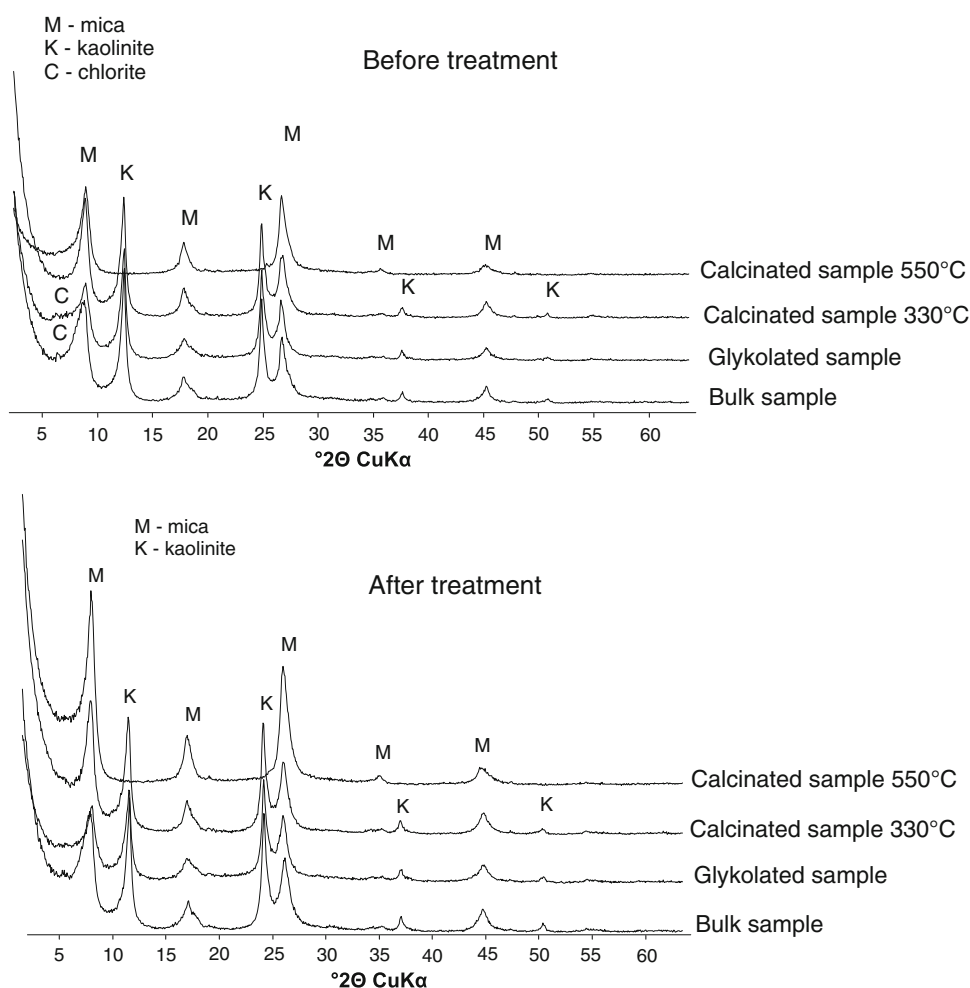
sis may not be fully reliable because of the small volume of the sample, which causes high background intensity and thus provides a poor diffraction pattern.

The mineral composition of the sediments accumulated at the bottom of the reactors due to the interaction experiments between brine, CO_2 and the rock for the different samples is shown in Table 4. The XRD analysis of those sediments showed well-defined XRD diffraction patterns, so the interpretation of mineral composition was reliable. The mineral composition of sediments proved that those minerals are derived from the rock samples.

4 Discussion

The experiments on the interaction between brine, CO_2 and reservoir and caprock samples were intended to show changes in the rocks that appear as a result of such reactions, and to answer the question whether and how such interactions affect the properties of reservoir (sandstones) and cap (carbonate) rocks.

It should be noted that studies of individual samples cut from drill cores (and especially those from rocks of highly variable mineral composition and porosity within a single sample) are not fully representative of the rocks (see [27]). Both interpretation and comparison of pre- and post-reaction samples should be performed with caution. Due to the considerable variability in the mineral composition and porosity, comparative studies should be carried out on at least four or five samples representing the same rock type. It should be borne in mind that the samples analysed before and after the experiment were not exactly the same samples, although the best efforts were taken to collect them from the same drill core intervals, if possible. Perhaps additional fluid chemistry might show greater changes for such experiments.

4.1 Textural Properties

Small variations in specific BET surface area values were observed (Fig. 9) in all of the CO_2-brine-treated rock samples analysed. The measured values for sandstone sample Nos. 2, 4, 7, 8 and limestone sample No. 1 increased after the experiment, while those measured for sandstone sample Nos. 3, 6 and dolostone sample No. 5 decreased. Most values of aver-
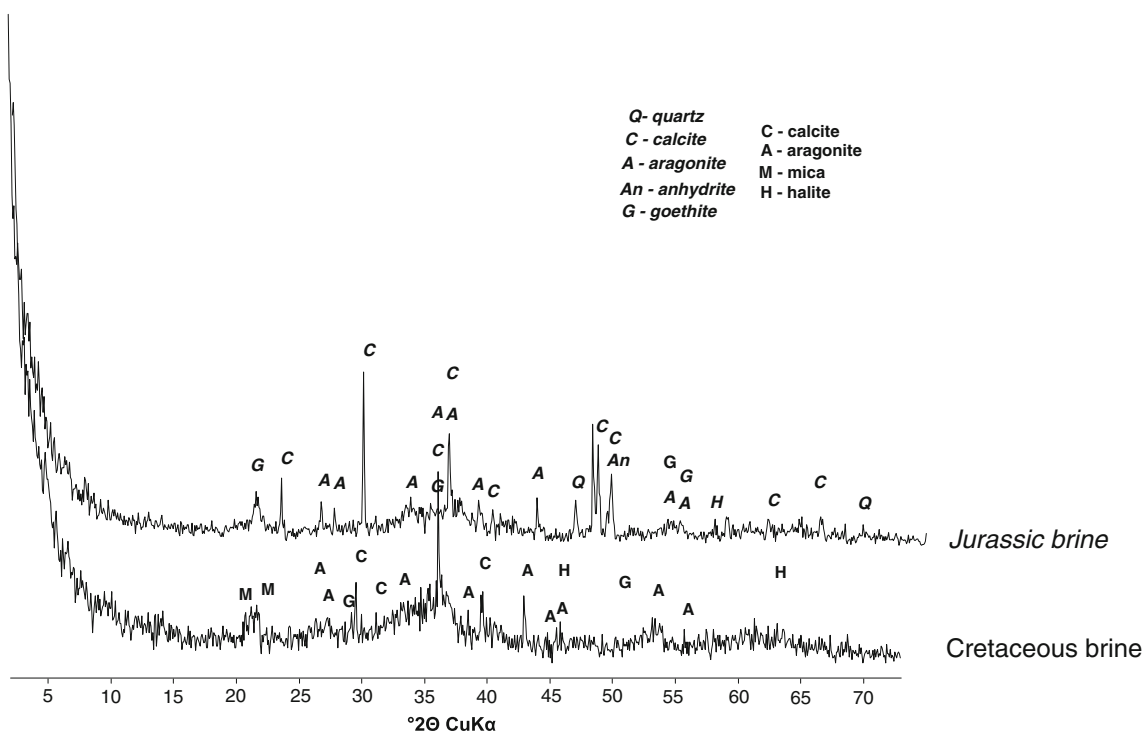
Fig. 8 X-ray diffraction pattern of the sediments accumulated due to reactions between Lower Cretaceous brine and CO_2, and Lower Jurassic brine and CO_2

Table 4 Sediments mineral composition accumulated at the bottom of the reactor

| Sample	Sediments mineral composition at the bottom of the reactor
No. 1	Calcite, aragonite, halite
No. 2	Quartz, calcite, halite
No. 3	Quartz, feldspars, halite
No. 4	Quartz, kaolinite, illite, goethite, halite
No. 5	Calcite, aragonite, strontianite, nacrite
No. 6	Quartz, feldspars, goethite, kaolinite, halite
No. 7	Quartz, mica, calcite, kaolinite
No. 8	Quartz, feldspars, jarosite

age pore diameter decreased after the tests (Fig. 9), except for sample No. 5 for which the value slightly increased.

As it was mentioned before, qualitative analysis of nitrogen adsorption and desorption isotherms showed that N_2 adsorption isotherms obtained for both sandstones and carbonates can be categorized as Type IV isotherms. The presence of micro/mesoporous structure of the sandstones and carbonates was indicated by both low values of specific surface area and small volume of pores at their relatively large diameters. The H3/H2 Type hysteresis loop in the isotherms of the studied materials, whose shape is related to the actual pore structure, starts at low relative pressure. This implies a

very small proportion of micropores in the structure of the rock material. The shape of the hysteresis loop corresponds to the presence of blind spherical and ink bottle-shaped pores.

The results obtained by these methods are very different. However it should be noted that most samples showed a slight reduction in pore size associated with a slight increase in the BET surface areas. This is associated with the before-mentioned accuracy of the measurements which depends on many factors: i.e. sample preparation, degassing, weighing, bath temperature stability, and purity of gases used in the analysis. A particular reason for variable results is a clear heterogeneity of analyzed samples. Therefore these analyses should be repeated at least four times for each sample depth interval and averages calculated.

4.2 Mineralogical and Petrographical Characterization

The sandstone samples were poorly cemented and hard to prepare for microscope analysis, therefore, full mineralogical characterization was limited. Referring to the previous works on this issue, the following reasons for the results can be inferred: (a) insufficient representativeness of the samples (see [28]), (b) too few reactive minerals (quartzose sandstones, and thus insufficient amount of feldspars reactive with CO_2 and carbonates with small amount of reactive clay minerals, and (c) short duration of the experiment (see [28,29]).

Fig. 9 Graphs of textural parameters before and after experiments; **a** the BET surface area, **b** average pore diameter
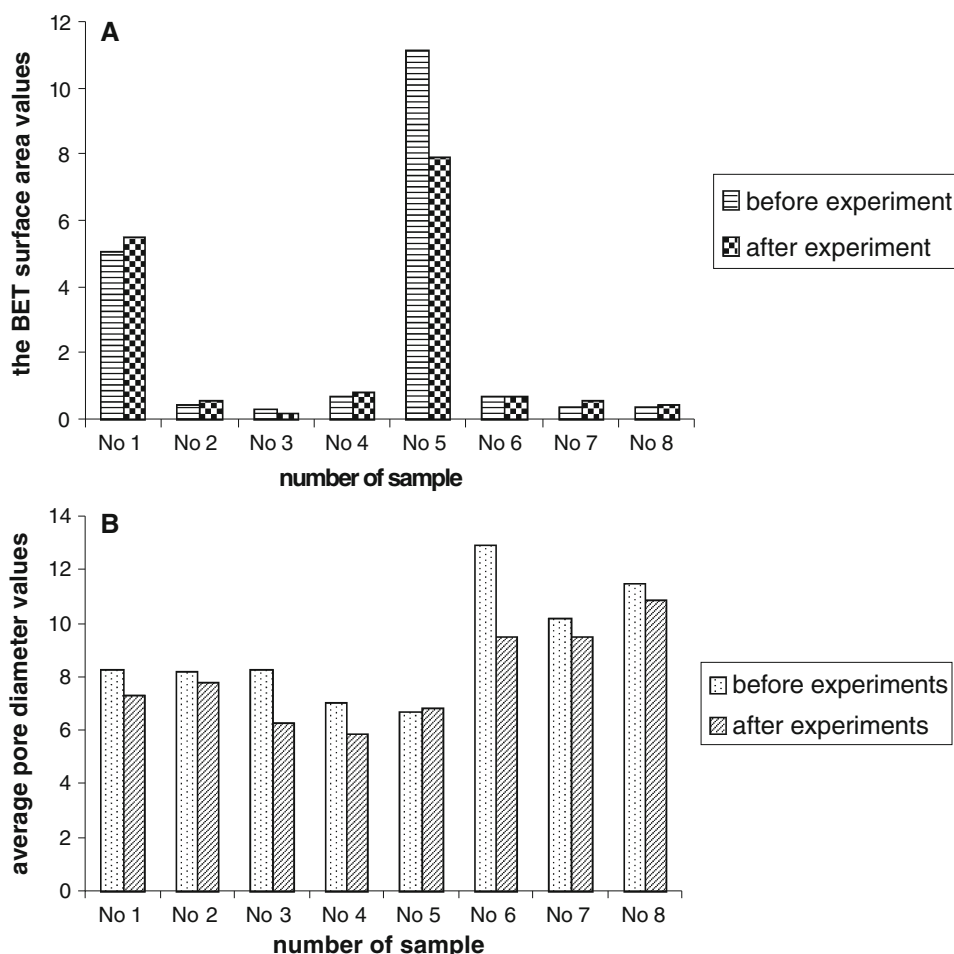
The samples after the experiments remained very similar to the corresponding samples before the experiment. The XRD analysis revealed that nearly all the samples (except for sample No. 5) contain neoformed halite. Its occurrence was caused by the crystallization of this mineral from saline solutions used in the experiments, because the samples were not washed after the experiments before drying them.

Interesting mineralogical results were obtained from sample No. 2. It showed an increase of cement quantity that is a mixed, interstitial and carbonate-clay (much of calcite). This sandstone has a porous character and contains glauconite. The composition of this sample changed after the experiment. The quantity of the carbonate cement decreased to nearly zero because of its dissolution in acidic, carbonated waters.

The analysis of the sediments formed at the bottom of the reactors during the blank experiments showed that the brine prepared for the Cretaceous samples was more reactive/aggressive than that prepared for the Jurassic samples. This conclusion is based on the presence of goethite that precipitated probably as a result of the effect of brine and CO_2 on the internal reaction vessel walls (i.e. corrosion of the reaction cells). This mineral was not observed in the X-ray diffraction patterns of the sediment accumulated from brine prepared for the Jurassic deposits. Moreover, the sediments of both brines contain carbonates that formed as a result of reaction between CO_2 and the brines. As the amount of the sediment was very small, XRD analysis yielded weak diffraction pattern with strongly increased background intensity (especially for Jurassic brine). Therefore, identification of any other minerals was not reliable.

XRD reflections obtained for the sediments accumulated as a result of the reaction between brine and Cretaceous samples (Nos. 1–4) are very sharp and reflect the composition of the rock sample involved in the test. Additionally, the XRD patterns reveal diffraction peaks associated with halite that is an artefact after drying of the sediments (that were not washed after the experiment).

XRD analyses of the sediments that formed after reaction of brine and Jurassic samples show slightly increased background intensity, probably because of the inappropriate parameters of measurement used for the small amount of analyzed material. In the case of rock sample No. 5, there are diffraction reflections related to carbonates (strontianite)

and nacrite, which are absent in the primary rock sample. In addition to quartz and feldspars, the sediment of rock sample No. 8 shows a distinct peak associated with jarosite.

5 Conclusions

The changes in textural parameters are highly variable and difficult to interpret. However, the results of the mineralogical-petrographic analyses showed that the effect of CO_2–brine–rock interaction in these experiments was very small, both on a macro- and micro-scale.

No new mineral phases formed in the experiments (except for halite that was observed in most of the sandstone samples). That said, the run conditions of the experiments were relatively benign, CO_2–water–(silicate)rock interactions were fairly slow, and the amounts of secondary phases formed might have been very small. We cannot rule out their presence at concentrations below the detection limits for the techniques used in this study.

After 3 months under near-formation conditions, the mineral composition of the rocks, as well as the surface parameters of the reservoir rock did not reveal any significant changes. The changes may be in part associated with the heterogeneity of analyzed samples as well as with possible errors introduced during the experiments, which may include sample preparation, degassing, weighing, bath temperature stability, and purity of gases used in the analysis.

Furthermore, some sediments (mainly carbonates) were found at the bottom of the reactor as a result of both the reaction between CO_2 and brine; and CO_2, brine and rocks. It should be noted however that another reason for the presence of these sediments could be the precipitation of carbonates as a result of fast degassing and depressurised CO_2-saturated and calcite-saturated solutions.

The results from this research suggest that short-term static experiments are not the ideal method to assess the textural and mineralogical-petrographic changes of the rocks, because of the low rates of some reactions at their low temperature. Thus, the results of this study based on static experiments provide only rough approximations of the brine–CO_2–rock interactions. A more appropriate method would be long-period flow experiments (see [29,30]), or conducted static short-term experiments should have a higher temperature in order to maximize the rates of silicate reactions within the time frame of the experiments [31,32].

References

1. IPCC: IPCC special report on carbon dioxide capture and storage. In: Metz, B.; Davidson, O.; de Coninck H.C.; Loos, M., Meyer, L.A. (eds.) Prepared by Working Group III of the Intergovernmental Panel on Climate Change, p. 442. Cambridge University Press, Cambridge (2005)
2. Zeidouni, M.; Pooladi-Darvish, M.; Keith D.: Analytical Solution to Evaluate Salt Precipitation during CO_2 Injection in Saline Aquifers. Energy Procedia **1**(1), 1775–1782 (2009)
3. Muller, N.; Qib, R.; Mackiea, E.; Pruessc, K.; Blunt, M. J.: CO_2 injection impairment due to halite precipitation. Energy Procedia **1**(1), 3507–3514 (2009)
4. Wollenweber, J.; Alles, S.; Kronimus, A.; Buschc Helge Stanjekd, A.; Krooss, B.M.: Caprock and overburden processes in geological CO_2 storage: An experimental study on sealing efficiency and mineral alterations. Energy Procedia **1**(1), 3469–3476 (2009)
5. Gaus, I.: Role and impact of CO_2–rock interactions during CO_2 storage in sedimentary rocks. Int. J. Greenhouse Gas Control **4**, 73–89 (2010)
6. Mahdavi, M.; Mahvi, A.H.; Nasseri, S.; Yunesian, M.: Application of freezing to the desalination of saline water. Arab. J. Sci. Eng. **36**(7), 1171–1177 (2011)
7. Maliva, R.G.; Missimer T.M.; Winslow F.P.; Herrmann R.: Aquifer storage and recovery of treated sewage effluent in the Middle East. Arab. J. Sci. Eng. **36**(1), 63–74 (2011)
8. Enick, R. M.; Lara, S. M.: CO_2 solubility in water and brine under reservoir conditions. Chem. Eng. Commun. **90**, 23–33 (1990)
9. Czernichowski-Lauriol, I.; Snajuan B.; Rochelle C.; Bateman K.; Pearce, J.; Blackwell P.: Analysis of the geochemical aspects of the underground disposal of CO_2. In: Tsang, C.; Apps J.A. (eds.) Deep Injection Disposal of Hazardous and Industrial Waste, pp. 565–583. Academic Press, New York (1996)
10. Gunter, W.D.; Perkins, E.H.; Mccann, T.J.: Aquifer disposal of CO_2-rich gases reaction design for added capacity. Energy Convers. Manag. **34**, 941–948 (1993)
11. Bertier, P.; Swennen, R.; Leanen, B.; Lagrou D.; Dreesen, R.: Experimental identification of CO_2–water–rock interactions caused by sequestration of CO_2 in Westphalian and Buntsandstein sandstones of the Campine Basin (NE-Belgium). J. Geochem. Explor. **89**(1–3), 10–14 (2006)
12. Gaus, I.; Azaroual M.; Czernichowski-Lauriol I.: Reactive transport modelling of the impact of CO_2 injection on the clayey caprock at Sleipner (North Sea). Chem. Geol. **217**, 319–337 (2005)
13. Tarkowski, R.; Manecki, M. (eds): Badania oddziaływania CO_2 na mezozoiczne skały zbiornikowe w celu okreœlenia ich przydatnoœci do geologicznej sekwestracji dwutlenku wêgla, IGSMiE PAN, Kraków (2009)
14. Tarkowski, R.; Uliasz-Misiak, B.: Struktury geologiczne (poziomy wodonośne i złoża węglowodorów) dla podziemnego składowania CO_2 w Polsce. In: Tarkowski, R., (ed.) Podziemne składowanie CO_2 w Polsce w głębokich strukturach geologicznych (ropo-, gazoi wodonoœnych), pp. 69–111. Publisher IGSMiE PAN, Kraków (2005)
15. Tarkowski, R.; Uliasz-Misiak, B.: Possibilities of CO_2 sequestration by storage in geological media of major deep aquifers in Poland. Chem. Eng. Res. Des **84**(A9), 776–780 (2006)

16. Tarkowski, R.: CO_2 storage capacity of geological structures located within Polish Lowlands' Mesozoic formations. Gosp. Sur. Miner.-Miner. Resour. Manag. **24**(4/1), 101–112 (2008)

17. Brosse, É.; Maginer C.; Vincent B.: Modelling fluid-rock interaction induced by the percolation of CO_2-enriched solutions in core samples:the role of reactive surface area. Oil Gas Sci. Technol. **60**(2), 287–305 (2005)

18. Tarkowski R.; Wdowin M.: Petrophysical and mineralogical researches on the influence of CO_2 injection on Mesozoic reservoir and caprocks from the Polish Lowland. Oil Gas Sci. Technol. **66**(1), 137–150 (2011)

19. Franus, W.; Wdowin, M.: Removal of ammonium ions by selected natural and synthetic zeolites. Gosp. Sur. Miner.-Miner. Resour. Manag. **26**(4), 133–148 (2010)

20. Gregg, S.J.; Sing, K.S.W.: Adsorption, Surface Area and Porosity. 2nd edn. Academic Press, London (1982)

21. Wdowin, M., Gruszecka, A.: Mineralogical-chemical and textural characteristics of Zn–Pb industry flotation wastes with further potential for application as sorbents (in polish). Gosp. Sur. Miner.-Miner. Resour. Manag. **28**(3), 55–69 (2012)

22. Jackson, M. L.: Soil chemical analysis—advanced course. 2nd edn. Published by the author, Dep. of Soil Science, Univ. of Wisconsin, Madison, WI (1969)

23. Moore, D.; Reynolds, R.: X-Ray diffraction and the identification and analysis of clay minerals. Oxford University Press, New York (1997)

24. IUPAC: Manual of Symbol and Terminology for Physicochemical Quantities and Units. Appendix II. Definitions, Terminology and Symbols in Colloid and Surface Chemistry. Part 1. Pure Appl. Chem. **31**(4), 579–638 (1972)

25. Klinik, J.: Tekstura porowatych ciał stałych. AGH—Ośrodek Edukacji Niestacjonarnej, Kraków (2000)

26. Brindley, G.W.; Brown, G.: Crystal Structure of clay Minerals and their X-ray identification. Mineralogical Society Monograph N° 5, London (1984)

27. Carles, P.; Bachadu, P.; Lasseur, E.; Berne, P.; Bretonnier, P.: Confining properties of carbonates dogger caprocks (Parisian Basin) for CO_2 storage purpose. Oil Gas Sci. Technol. **65**(3), 461–472 (2010)

28. Nightingale, M.; Johnson, G.; Shevalier, M.; Hutcheon, I.; Perkins, E.; Mayer, B.: Impact of Injected CO_2 on Reservoir Mineralogy During CO_2-EOR. Energy Procedia **1**(1), 3399–3406 (2009)

29. Credoz, A.; Bildstein, O.; Jullien, M.; Rayn, J.; Pétronin, J. C.; Lillo, M.; Pozo, C.; Geniaut, G.: Experimental and modeling study of geochemical reactivity between clayey caprocks and CO_2 in geological storage conditions. Energy Procedia **1**(1), 3445–3452 (2009)

30. Fisher, S.; Liebscher, A.; Wandrey, M.: The CO_2 SINK group: CO_2–brine–rock interaction—first result of long-term exposure experiments at in situ P-T conditions of the Ketzin CO_2 reservoir. Chem. Erde-Geochem, **70**(S3), 155–164 (2010)

31. Huq, F.; Blum, P.; Marks, M.A.W.; Nowak, M.; Haderlein, S.B.; Grathwohl, P.: Chemical changes in fluid composition due to CO_2 injection in the Altmark gas field: preliminary results from batch experiments. Environ. Earth Sci. **67**(2), 385–394 (2012)

32. Liu, F.; Lu, P.; Griffith, C.; Hedges, S.W.; Soong, Y., Hellevang, H.; Zhu, Ch.: CO_2–brine–caprock interaction: reactivity experiments on Eau Claire shale and a review of relevant literature. Int. J. Greenhouse Gas Control **7**, 153–167 (2012)